AGU PUBLICATIONS

JGR

Journal of Geophysical Research: Earth Surface

RESEARCH ARTICLE
10.1002/2014JF003224

Key Points:
- MMI, tectonics, and topography control coseismic landslide occurrence
- The modeling approach incorporates fuzzy set theory in GIS
- The model requires no site-specific data inputs to perform the assessment

Correspondence to:
T. Kritikos,
theo.kritikos@gmail.com

Citation:
Kritikos, T., T. R. Robinson, and T. R. H. Davies (2015), Regional coseismic landslide hazard assessment without historical landslide inventories: A new approach, *J. Geophys. Res. Earth Surf.*, *120*, 711–729, doi:10.1002/2014JF003224.

Received 28 MAY 2014
Accepted 24 FEB 2015
Accepted article online 26 FEB 2015
Published online 13 APR 2015

Regional coseismic landslide hazard assessment without historical landslide inventories: A new approach

Theodosios Kritikos[1], Tom R. Robinson[1], and Tim R. H. Davies[1]

[1]Department of Geological Sciences, University of Canterbury, Christchurch, New Zealand

Abstract Currently, regional coseismic landslide hazard analyses require comprehensive historical landslide inventories as well as detailed geotechnical data. Consequently, such analyses have not been possible where these data are not available. A new approach is proposed herein to assess coseismic landslide hazard at regional scale for specific earthquake scenarios in areas without historical landslide inventories. The proposed model employs fuzzy logic and geographic information systems to establish relationships between causative factors and coseismic slope failures in regions with well-documented and substantially complete coseismic landslide inventories. These relationships are then utilized to estimate the relative probability of landslide occurrence in regions with neither historical landslide inventories nor detailed geotechnical data. Statistical analyses of inventories from the 1994 Northridge and 2008 Wenchuan earthquakes reveal that shaking intensity, topography, and distance from active faults and streams are the main controls on the spatial distribution of coseismic landslides. Average fuzzy memberships for each factor are developed and aggregated to model the relative coseismic landslide hazard for both earthquakes. The predictive capabilities of the models are assessed and show good-to-excellent model performance for both events. These memberships are then applied to the 1999 Chi-Chi earthquake, using only a digital elevation model, active fault map, and isoseismal data, replicating prediction of a future event in a region lacking historic inventories and/or geotechnical data. This similarly results in excellent model performance, demonstrating the model's predictive potential and confirming it can be meaningfully applied in regions where previous methods could not. For such regions, this method may enable a greater ability to analyze coseismic landslide hazard from specific earthquake scenarios, allowing for mitigation measures and emergency response plans to be better informed of earthquake-related hazards.

1. Introduction

Large earthquakes in mountainous environments result in a wide range of secondary hazards which can significantly increase the event impacts. Among the most notable of these effects are the various types of slope failure that can result in long-term (multidecadal) geomorphic and socioeconomic impacts [*Hewitt et al.,* 2008; *Robinson and Davies,* 2013]. Coseismic landslide hazard, defined herein as the relative probability of landslide occurrence at a specific location in a specific event, is a function of intrinsic slope characteristics (slope angle, material strength, lithology, etc.), which dictate the susceptibility to failure and do not change appreciably with time, and of strong ground motion from earthquakes, which acts as the triggering factor [e.g., *Meunier et al.,* 2007]. In recent earthquakes, such as the 1999 Chi-Chi and 2008 Wenchuan events, tens of thousands of landslides occurred affecting areas of several thousands of square kilometers [*Dadson et al.,* 2004; *Dai et al.,* 2010; *Gorum et al.,* 2011]. Understanding and modeling the factors influencing coseismic slope failures is necessary to develop effective hazard and risk assessment methods to underpin mitigation plans.

Since the first models of the effects of seismic shaking on slope stability in the 1950s [*Terzhagi,* 1950], various methods have been proposed to assess the stability (or performance) of slopes during earthquakes. Commonly applied methods are pseudostatic analysis [*Stewart et al.,* 2003; *Bray and Travasarou,* 2009], stress-deformation analysis (finite element model) [*Clough and Chopra,* 1966], and permanent-displacement analysis (Newmark displacement model) [*Newmark,* 1965; *Jibson et al.,* 2000]. These are primarily applicable to specific slopes although the Newmark displacement model has been adapted for more regional studies [*Jibson,* 2007; *Saygili and Rathje,* 2008; *Rathje and Antonakos*, 2011; *Rathje and Saygili*, 2009]. Statistical methods using geographic information systems (GIS) have also been successfully utilized for regional landslide hazard assessments [*Van Westen et al.,* 1997; *Aleotti and Chowdhury*, 1999; *Guzzetti et al.,* 1999; *Huabin et al.,* 2005; *Crozier and Glade*, 2005].

These are useful at regional scales because they are objective, reproducible, easy-to-update, and can have fewer data requirements than physical modeling approaches [*Naranjo et al.,* 1994; *Soeters and Van Westen*, 1996; *Van Westen et al.,* 2006; *He and Beighley,* 2008]. Statistical methods are based on relationships between known historical landslide locations and various causative factors [*Remondo et al.,* 2003a], assuming that future slope failures are likely to occur under similar conditions [*Varnes and IAEG Commission on Landslides and other Mass-Movements,* 1984; *Carrara et al.,* 1991, 1995; *Guzzetti et al.,* 1999; *Dai and Lee*, 2002]. This enables those factors that are common to all studied slope failures to be identified and utilized for regional analysis.

Several statistical methods exist for modeling regional-scale coseismic landslide hazard [e.g., *Lee et al.,* 2008; *Miles and Keefer,* 2000, 2007, 2009a, 2009b; *Jibson et al.,* 2000]. These can be highly successful for the areas in which they are trained, but very few have been applied beyond their training area. Typically, these methods incorporate predisposing factors such as slope angle and height, vegetation cover, soil depth, moisture content, terrain roughness, soil or rock strength index, horizontal distance to streams or roads, etc., with modified Mercalli (MM) shaking intensity or peak ground acceleration (PGA) as the triggering factor [*Miles and Keefer,* 2007, 2009a; *Lee et al.,* 2008; *Jibson et al.,* 2000]. As a result, these methods require (i) a comprehensive and accurate landslide inventory, (ii) multiple strong motion recordings or detailed isoseismals, (iii) accurate geologic maps, (iv) extensive geotechnical data, and (v) accurate digital elevation models (DEMs) [*Harp et al.,* 2011; *Jibson et al.,* 2000]. However, in many regions neither comprehensive landslide inventories nor extensive geotechnical data are available. As a result, very few methods exist [e.g., *Del Gaudio et al.*, 2003; *Del Gaudio and Wasowski,* 2004] for regional-scale assessment of coseismic landslide hazard for such areas, and this is a top research priority [*Wasowski et al.,* 2011].

Herein we describe a new approach to coseismic landslide hazard analysis for specific earthquake scenarios, in regions without historical landslide inventories or detailed geotechnical data. This is based on the concept of fuzzy logic in GIS, applied in previous studies [*Miles and Keefer*, 2007, 2009a; *Lee et al.,* 2008]. The factors controlling landslide occurrence are deduced from statistical analysis of landslide inventories from the 1994 Northridge and 2008 Wenchuan earthquakes and are applied to the 1999 Chi-Chi earthquake to test the model's predictive performance beyond its training region. We first describe the concept of fuzzy logic and its application to landslide hazard modeling, before outlining the data used to derive and test the model. We then present an analysis of the factors influencing landslide occurrence in Northridge and Wenchuan and use these to model landslide hazard in each event. Finally, we provide a sensitivity analysis of the results before applying the memberships to Chi-Chi to test the model's success beyond the training environments.

2. Method

2.1. Fuzzy Set Theory

Landslide hazard analysis requires generalizations and simplifications of complex physical processes. Fuzzy logic is a method of modeling highly complex systems that deals with uncertainties related to insufficient knowledge, data limitations, and ambiguous or imprecise input information [*Zadeh*, 1965]. Fuzzy logic derives from fuzzy set theory which is an extension of classical set theory [*Ross*, 1995]. In classical set theory, an element has a clearly defined relationship with a set, which means that the element either belongs (1) or does not belong (0) to the set; therefore, its membership degree value can be either 0 or 1.

$$\chi_A(x) = \begin{cases} 1, & x \in A \\ 0, & x \notin A \end{cases} \tag{1}$$

where $\chi_A(x)$ is the characteristic function of element x representing the membership of x in the set A. Fuzzy logic is based on the concept of partial membership, where elements have varying degrees of membership between 0 and 1:

$$\{\mu_A(x) \in \mathbb{R} \,|0 \le x \le 1|\} \tag{2}$$

where $\mu_A(x)$ is the membership function—the degree of membership of the element in the fuzzy set. A value of 1 indicates full membership, 0 indicates no membership, and all real values between 0 and 1 are possible.

Membership functions can be either user defined (based on subjective judgment to determine the relative importance of the predictive variables), data driven, or a combination. These can be derived by various functions, such as J-shaped, S-shaped, triangular, trapezoidal, or linear, that represent different relationships

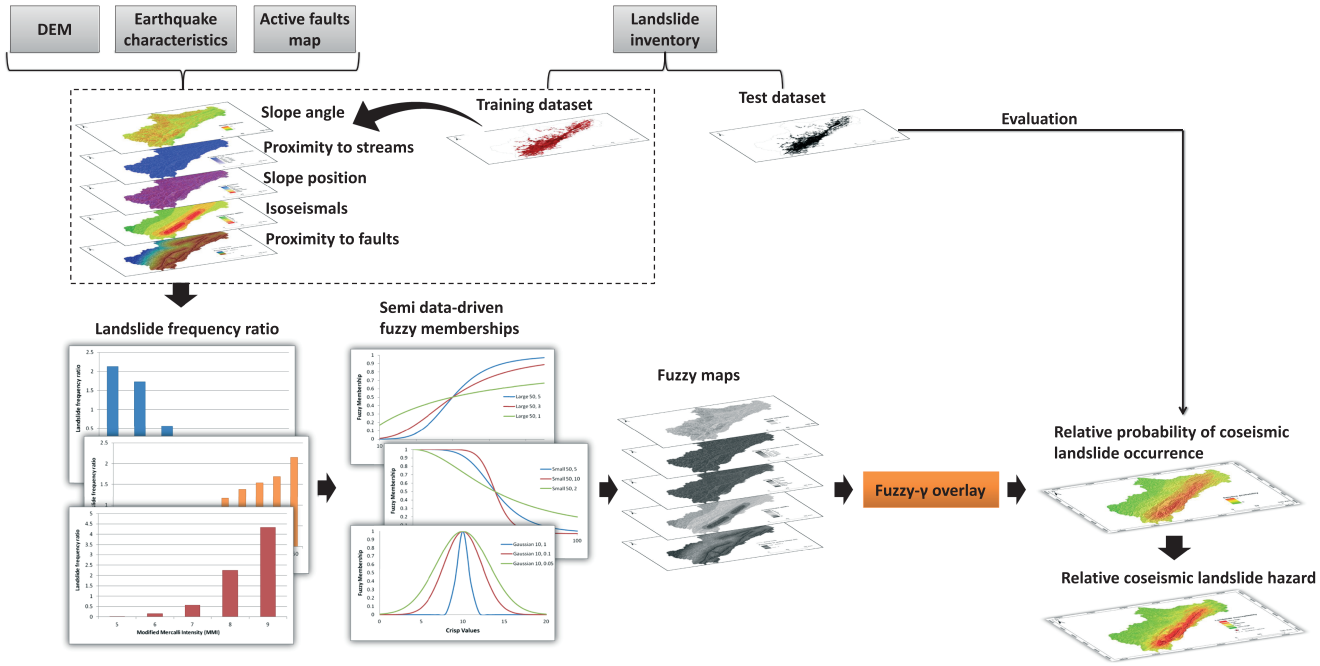

Figure 1. Illustrative workflow of the fuzzy logic method for coseismic landslide hazard assessments.

between factors and the phenomena being studied [*Bonham-Carter,* 1994; *Wang et al.,* 2009]. This study utilizes semi data-driven memberships from a series of functions available in Environmental Systems Research Institute's ArcGIS. In order to minimize issues associated with subjectivity, the shapes of the membership curves are fitted to landslide densities from the inventory data using the coefficient of determination (R^2). However, some curves are subsequently manually altered to account for known errors and inconsistencies within the data.

The density of landslides is calculated from the frequency ratio, i.e., the relative frequency of landslides within a factor compared with the relative frequency of landslides in the entire study area [e.g., *Lee and Pradhan,* 2007; *Lee and Sambath*, 2006; *Yilmaz*, 2009]:

$$\text{Frequency ratio} = \frac{N_{(Li)}/N_{(Ci)}}{N_{(L)}/N_{(A)}} \tag{3}$$

where $N_{(Li)}$ is the number of landslide pixels in the factor i, $N_{(Ci)}$ is the total number of pixels in the factor i, $N_{(L)}$ is total number of landslide pixels in the study area, and $N_{(A)}$ is the total number of pixels of the study area.

2.2. Fuzzy Overlay

GIS-based landslide hazard analyses require the combination of various factors in the form of spatial layers to develop the final hazard map. When all relevant factors have been transformed into fuzzy membership data sets, these are aggregated together to produce a final fuzzy set describing the landslide hazard (Figure 1) [*Dubois and Prade*, 1985; *Zimmermann*, 1991]. This stage requires the user to decide how the factors are combined in order to produce a meaningful output. Different operators are available such as *fuzzy AND*, *fuzzy OR*, *fuzzy Product*, *fuzzy Sum*, and *fuzzy Gamma* [*Bonham-Carter,* 1994]. The fuzzy AND and fuzzy OR operators are used to identify the lowest and highest membership values, respectively, for each pixel within all the membership data sets. They are therefore useful for identifying either the most or least influencing factor for any given pixel but not the effect of multiple combined factors. The fuzzy Sum and fuzzy Product operators assume that by combining factors, the resulting hazard/pixel value is either larger or smaller, respectively, than each of the individual membership sets. These operators are rarely used as they do not sufficiently represent the effect of multiple combined influencing factors [*Environmental Systems Research Institute*, 2011].

The fuzzy Gamma operator is a compromise and effectively establishes the combined effect of multiple memberships on the final hazard such that

$$\mu_{(x)} = \left(\prod_{i=1}^{n}\mu_i\right)^{1-\gamma} \cdot \left(1 - \prod_{i=1}^{n}(1-\mu_i)\right)^{\gamma} \quad (4)$$

where $\mu_{(x)}$ is the combined membership value (or hazard), μ_i is the fuzzy membership function for factor *i,* where $i = 1, 2, \ldots, n$ is the number of memberships to be combined, and γ is a user-defined parameter between 0 and 1. The γ value establishes the effect of large μ_i values (i.e., those favoring the occurrence of landslides) compared to small μ_i values (i.e., those discouraging the occurrence of landslides). A large γ assigns greater influence to favorable μ_i values in the final output, while a small γ assigns greater influence to unfavorable μ_i values. The optimum γ for hazard assessments must achieve high hazard for known landslide locations across an area not significantly larger than the total landslide affected area.

3. Data

In this study coseismic landslide inventories from three historic earthquakes are used: 1994 Northridge (California), 2008 Wenchuan (China), and 1999 Chi-Chi (Taiwan). Below is a brief summary of these earthquakes, their tectonic environments, and the landslide inventories available.

3.1. 1994 M_w6.7 Northridge Earthquake

The Northridge earthquake occurred 30 km north of the Los Angeles basin beneath the city of Northridge in the San Fernando Valley, Southern California (Figure 2), at a focal depth of 18 km on a blind thrust fault [*Wald and Heaton*, 1994]. Slip occurred along a 14 km long section of the fault and reached a maximum of ~4 m with average slip measuring ~1.2 m. The region has a large number of mapped active faults and is within 100 km of the plate boundary San Andreas fault (Figure 2). Consequently, the region has high seismicity with $15 > M4.8$ earthquakes occurring in the greater Los Angeles area between 1920 and 1994 [*Hauksson et al.,* 1995]. In the Northridge earthquake, high shaking intensities occurred in the surrounding Santa Susana, Santa Monica, and San Gabriel Mountains (Figure 2), and >11,000 landslides were triggered across a total area ~10,000 km^2, up to 70 km from the epicenter [*Harp and Jibson*, 1996]. A distinct 1000 km^2 zone northwest of the epicenter represents the region of most concentrated landsliding (Figure 2). An inventory containing 11,111 landslides was compiled immediately after the event using field studies and aerial reconnaissance [*Harp and Jibson*, 1996]. On sunlit slopes, landslides as small as 1–2 m across were easily identifiable; however, on shadowed slopes only landslides 5–10 m across or larger could be identified. Field observations suggested that landslides occurred dominantly on south facing slopes, which are sunlit in the aerial photography; thus it is thought >80% of landslides >5 m across have been mapped [*Harp and Jibson*, 1996]. Landslides were mapped as polygons and manually digitized via GIS on 1:24,000 scale base maps. Mapping errors were estimated to be no more than 30 m [*Harp and Jibson*, 1996]. Herein, the polygon data are converted to top point (i.e., a point at the highest elevation of the polygon) to conform with data from the other inventories (Table 1).

3.2. 2008 M_w7.9 Wenchuan Earthquake

The Wenchuan earthquake occurred in the Longmen Shan Mountains of Sichuan Province, eastern China (Figure 2). The causative Yingxiu-Beichuan fault is one of three major faults in the Longmen Shan fault zone which accommodate both dip-slip and dextral strike-slip motion [*Densmore et al.,* 2007]. As a result, the earthquake involved oblique thrust motion along a >320 km northwest dipping fault [*Xu et al.,* 2009]. Rupture originated at a focal depth of 14–19 km and propagated toward the northeast, with surface rupture along the entire rupture length and maximum vertical and dextral displacements of 6.2 m and 4.5 m, respectively [*Liu-Zeng et al.,* 2009; *Gorum et al.,* 2011]. Prior to 2008, only 66 major earthquakes were known to have occurred in the region since 638 A.D., the largest of which was M_s7.2 in 1976 [*Li et al.,* 2009].

The Longmen Shan Mountains are characterized by extreme relief with elevations up to 7500 m above sea level. The earthquake caused very strong ground shaking along the full length of the fault rupture and within the ranges (Figure 2). As a result >60,000 landslides were triggered across a total area of 35,000 km^2 with the most concentrated zone covering ~8000 km^2 [*Gorum et al.,* 2011]. More than 200 landslide dams were reported [*Cui et al.,* 2009], although more recent work suggests there may have been >800 [*Fan et al.,* 2012]. Following the earthquake, numerous studies of the consequential landsliding were undertaken, and various

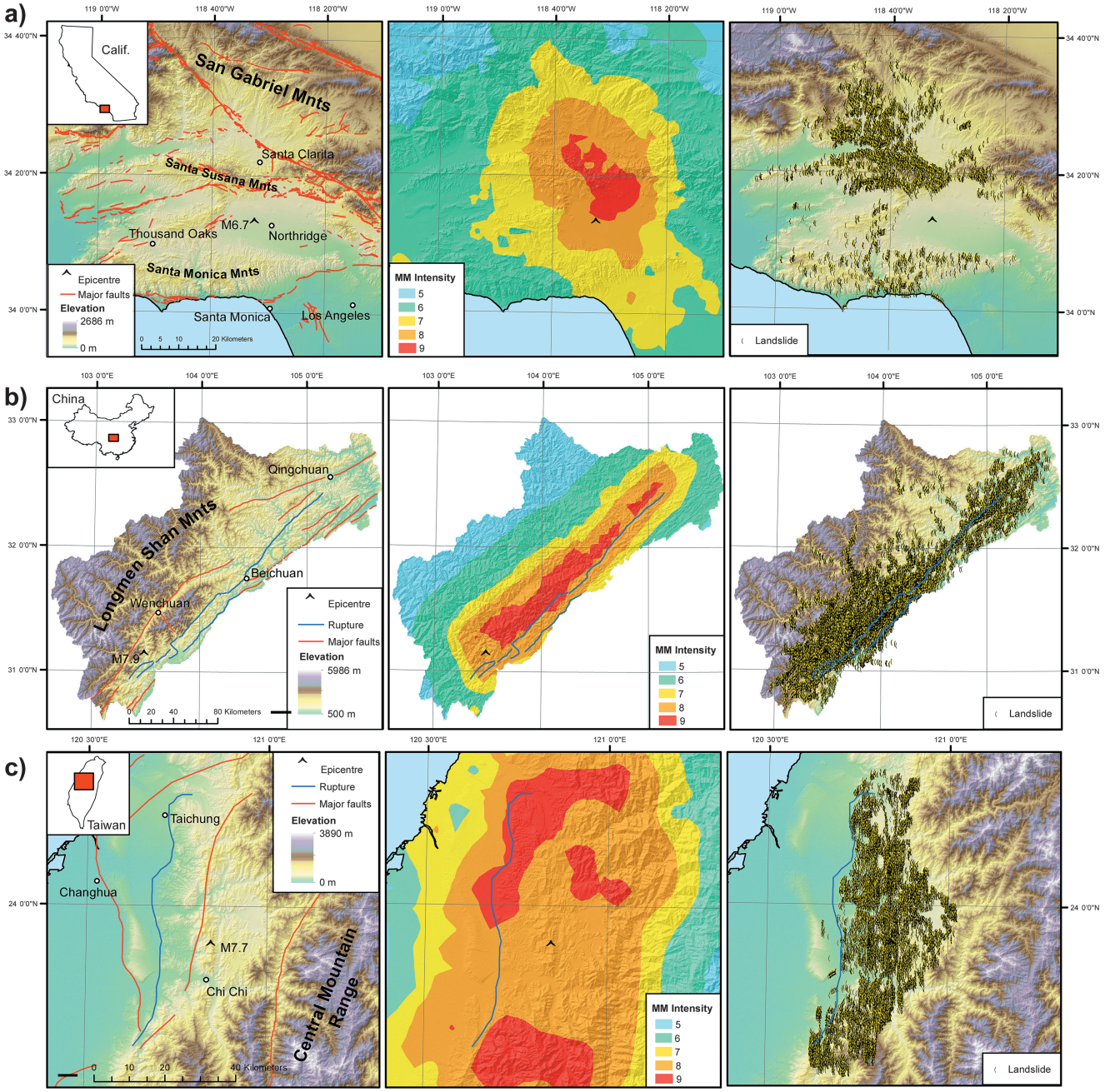

Figure 2. Maps showing the topography and mapped active faults, shaking intensity (from USGS, 2014), and mapped coseismic landslides for the (a) Northridge, (b) Wenchuan, and (c) Chi-Chi earthquakes. Landslide inventories are from http://pubs.usgs.gov/of/1995/ofr-95-0213/downloads/ (Northridge), *Gorum et al.* [2011] (Wenchuan), and Professor Hongey Chen of the National Taiwan University (Chi-Chi).

coseismic landslide inventories have been compiled [e.g., *Parker et al.*, 2011; *Gorum et al.*, 2011; *Li et al.*, 2014]. For the present study the inventory of *Gorum et al.* [2011] is used, which includes 60,109 landslides (Figure 2), identified from high-resolution (<15 m) satellite images and air photos. The images cover the entire affected region with 0.5% of the study region affected by cloud cover. Landslides were mapped as top points with a minimum resolvable source area of 600 m^2 [*Gorum et al.*, 2011]. It is not known what percentage of the total landslides is missing from this inventory; however, other inventories suggest similar numbers (~56,000: *Parker et al.* [2011] and ~57,000: *Li et al.* [2014]). Location accuracy for landslide points is thought to be similar to the pixel size of the satellite images used (i.e., ~15 m).

Table 1. Summary of Relevant Information on the Landslide Inventories From the 1994 Northridge, 2008 Wenchuan, and 1999 Chi-Chi Earthquakes

	Northridge	Wenchuan	Chi-Chi
Number	11,111	60,109	21,969
Coverage	>80% (larger than minimum size)	Unknown, assumed majority	Unknown, assumed majority
Inventory type	Top points (converted from polygons)	Top points	Top points (converted from polygons)
Minimum landslide size	5 m (width)	600 m^2 (source zone)	3600 m^2 (source and deposit)
Mapping error	<30 m	<15 m	<20 m
Mapping method	Aerial photographs and field studies	Pre-earthquake and postearthquake satellite images	Pre-earthquake and postearthquake satellite images

3.3. 1999 M_w7.7 Chi-Chi Earthquake

The Chi-Chi earthquake was centered 7.5 km beneath the town of Chi-Chi, central Taiwan. The earthquake had a complex source, rupturing over 100 km along the Chelungpu fault in a series of jumping dislocations [*Shin and Teng*, 2001]. The rupture surface was nonplanar following the surface expression of the fault with numerous changes in strike (Figure 2). Thrust motion predominated with maximum surface displacements of ~8 m; however, the complex fault trace resulted in multiple styles of motion including oblique slip [*Chi et al.*, 2001; *Shin and Teng*, 2001]. The region has an extremely high seismicity rate with at least 17 damaging earthquakes occurring during the twentieth century [*Yu et al.,* 1997].

The Chelungpu fault marks the boundary between the Central Mountains of Taiwan and the coastal plains (Figure 2). The 1999 earthquake generated strong shaking affecting a large region within the Central Mountains resulting in >20,000 landslides (Figure 2), the majority occurring across a 3000 km^2 region [*Dadson et al.,* 2004]. Most of the landslides were shallow debris slides [*Lin et al.,* 2004] although two large-volume rock avalanches resulted in 78 fatalities [*Chigira et al.,* 2003]. Herein the landslide inventory presented in *Dadson et al.* [2004] is used, which contains 21,969 landslide polygons (converted to top points) identified from 20 m resolution satellite images. Landslides >3600 m^2 are resolved, and other inventories contain similar numbers (~20,000: *Wang et al.* [2002]) suggesting that the majority of the total landslides is included. Location errors for mapped landslide polygons are similar to the pixel size of the satellite imagery (~20 m).

4. Inventory Analysis and Model Design

Previous coseismic landslide hazard models [e.g., *Miles and Keefer,* 2007, 2009a; *Jibson et al.,* 2000] have used historical inventories from a study area assuming the factors identified will have a similar influence in this area during the next event. However, accurate and complete inventories only exist for very few locations [*Xu*, 2014], so this approach is impossible for regions without historical inventories. Nevertheless, many of the same factors have been identified in previous studies (e.g., slope angle, distance from streams, shaking intensity) despite being from different study areas [e.g., *Miles and Keefer*, 2007, 2009a; *Gorum et al.,* 2011; *Lee et al.,* 2008]. The present approach shows that the effect of various factors on landslide occurrence is similar in different regions, allowing meaningful hazard analysis in regions without historical inventories. To achieve this, we identify a series of factors that play similar roles in influencing slope stability in the Northridge and Wenchuan landslide inventories. These factors are integrated using GIS-based fuzzy logic to derive average membership curves that can be applied beyond the training region. To ensure each of the derived factors is necessary for modeling, we then undertake a sensitivity analysis to evaluate the effect of each individual factor on predicting coseismic landslide hazard. Finally, the model is applied to the Chi-Chi earthquake (for which no statistical analysis is undertaken) in order to confirm its applicability beyond the Northridge and Wenchuan environments.

4.1. Training Stage

Initially, the Northridge and Wenchuan landslide inventories are randomly split into two datasets (training and test datasets), each containing half of the recorded landslides. Landslides for each set are selected using Hawth's Analysis Tools for ArcMap v.9.3 [*Beyer*, 2004] to avoid spatial clustering and ensure that both sets contain landslides from across the entire study area. The training data set is utilized to derive the frequency ratio of landslides within the various factors examined. This allows a direct comparison of each factor across both inventories. The test data set is used in the model evaluation to test the success of converting these

frequency ratios into fuzzy memberships (see below). This splitting ensures that the model is tested against its predictive ability, rather than its goodness of fit with the statistically analyzed training data.

The factors evaluated are selected from those previously identified in the literature: PGA, MM, slope angle, slope aspect, slope curvature, slope position, distance from mapped active faults, and distance from streams (or disturbance distance) [*Miles and Keefer*, 2007, 2009a]. Both PGA and MM are evaluated to identify which measure can best be used as the triggering factor. Only those factors with qualitatively similar frequency ratio distributions across both Northridge and Wenchuan are used for modeling; those with contrasting distributions are discarded. Contrary to bivariate statistical methods, the fuzzy logic model applied herein does not assume the conditional independence of the landslide causative factors. Therefore, the conditional independence has not been assessed using statistical tests such as that proposed by *Agterberg and Cheng* [2002]. However, the factors have been selected to ensure that they will not overestimate the relative probabilities of landside occurrence when combined. For example, ground shaking intensity decreases with distance from epicenter/rupture and therefore is intrinsically linked to PGA and MM. Thus, distance from epicenter/rupture is not investigated.

4.1.1. Triggering Factor

The triggering factor for coseismic landslides is the effect of strong ground shaking on a rock mass. Ground shaking is commonly quantified directly in terms of the maximum accelerations (PGA) or indirectly in terms of intensity (e.g., MM). Both PGA and MM are investigated in this study, with data obtained from the *USGS earthquake database* (http://earthquake.usgs.gov/) to identify which provides the best predictive ability. Similar frequency ratio distributions are observed for MM, however not for PGA; Wenchuan demonstrated increasing frequency ratio with PGA while Northridge demonstrated a Gaussian distribution (Figure 3). In both earthquakes the lowest intensity inducing landslides is MM V in accordance with numerous observations from other historic events [e.g., *Keefer*, 1984]. As intensity increases, to a maximum of MM IX in both events, the frequency ratio increases at similar rates (Figure 3). MM is therefore used as the triggering factor herein instead of PGA as it is strongly correlated in both events.

4.1.2. Predisposing Factors

Predisposing factors are the intrinsic characteristics that make a slope susceptible to failure and are generally unchanging with time [*Glade and Crozier*, 2005]**.** These factors combine with the triggering factor to generate landslide hazard. Herein the predisposing factors investigated are primarily topographic, as topography can readily be compared across multiple environments. An accurate DEM is therefore a key component of the analysis. Ensuring the DEMs used are of the same resolution is vital to ensure consistent modeling of data. Herein the Advanced Spaceborne Thermal Emission and Reflection Radiometer 60 m DEMs have been used for Northridge and Chi-Chi and a 60 m DEM from *Gorum et al.* [2011] for Wenchuan.

4.1.2.1. Slope Angle

Slope angle is considered to be the most critical predisposing factor in mass movement initiation regardless of triggering factor [*Jibson et al.,* 2000]. The greater downslope component of gravity at steeper slopes results in increased gravity-induced shear stress in the soil and rock, increasing its susceptibility to failure. Steep slopes that are exposed to sufficient shaking intensity are therefore anticipated to experience a higher degree of landsliding than shallow slopes, or steep slopes that experience less severe shaking. This is observed in both Northridge and Wenchuan, with frequency ratios generally increasing with slope angle (Figure 3). However, the Northridge frequency ratio noticeably decreases on slopes above 45°. A similar reduction in landslide occurrence at steeper slopes was found by *Khazai and Sitar* [2004] who observed a reduction of landslide percentage for slopes $>40°$ and *Parise and Jibson* [2000] who observed a significant decrease of landslide density for slopes $>50°$. This is likely because only a very small percentage of the total Northridge area with slope angles $>45°$ experienced MM VII or higher shaking (Figure 4). By comparison, Wenchuan had a larger percentage of slopes $>45°$ in MM VII or higher zones (Figure 4). The reduction in frequency ratio in Northridge on these slope angles is therefore more likely a result of the triggering factor rather than the slope angle itself. Hence, both events can be considered to show good correlation (Figure 3).

The slope is classified using 5° intervals up to 50°, in order to take into account the effect of small slope changes on slope stability and at the same time avoid using a large number of classes. Although the $>50°$ class groups a wide range of slope values into a single category, it is considered appropriate as it only covers 1.6% of Wenchuan and 0.02% of Northridge study areas.

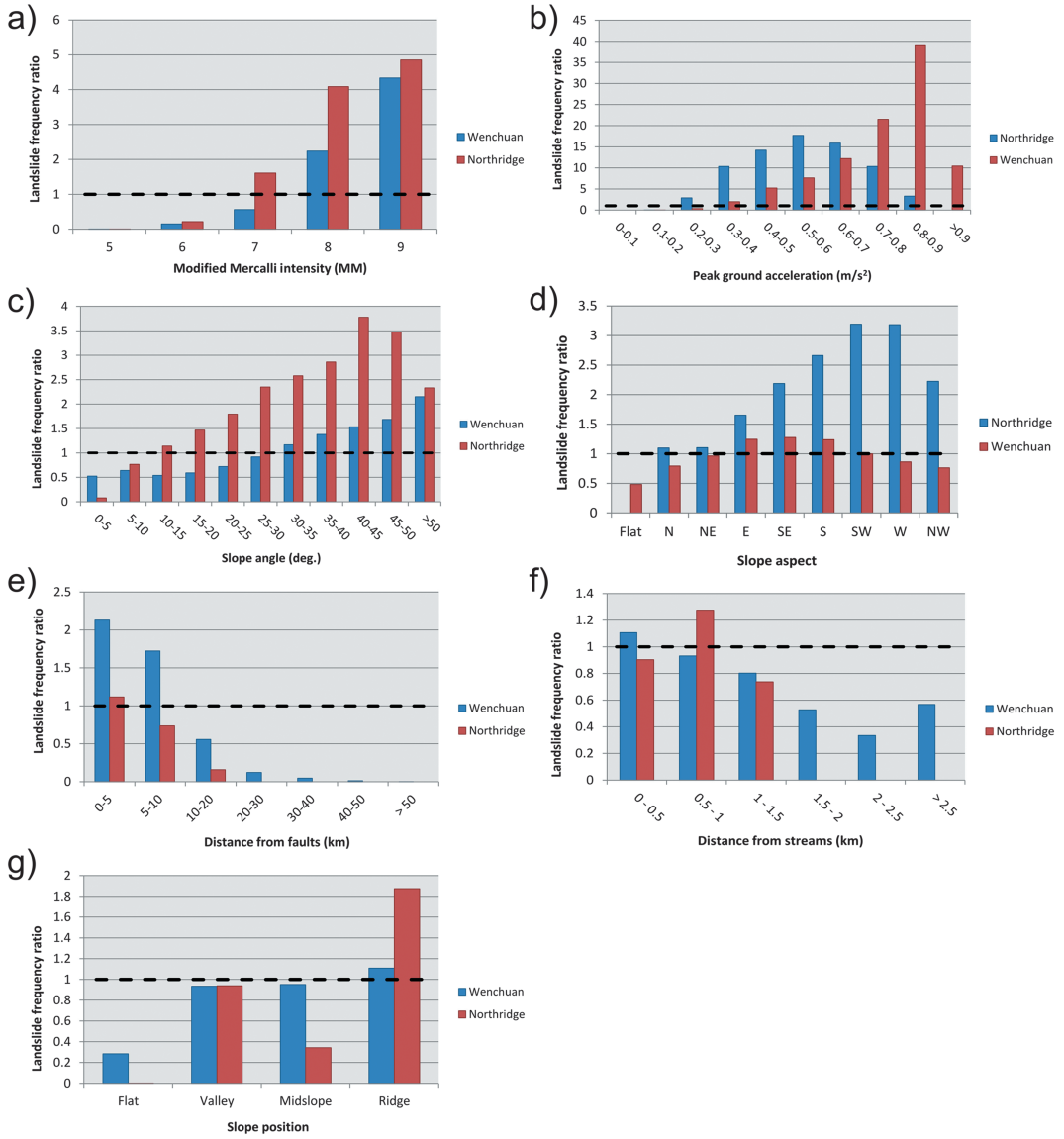

Figure 3. Landslide frequency ratio for (a) MM, (b) PGA, (c) slope angle, (d) slope aspect, (e) distance from active faults, (f) distance from streams, and (g) slope position. Horizontal dashed lines show frequency ratio of 1.

4.1.2.2. Proximity to Mapped Active Faults

The presence of active faults generally reduces the strength of the rock mass primarily by damage during previous earthquakes [*Dramis and Sorriso-Valvo*, 1994; *Brune*, 2001; Kellogg, 2001] as well as various other weakening mechanisms such as fault-related gully/slip systems [*Korup*, 2004] or groundwater infiltration and geochemical alterations [*Warr and Cox*, 2001]. This effect typically occurs within a few kilometers of the fault and results in the material being primed for failure by subsequent earthquakes, rainfall, or human activities [*Petley*, 2012]. Herein, distance from mapped active faults is computed using horizontal distances from the faults shown on published maps. The distances from active faults are classified using class sizes of 5 km and 10 km. The selection of class intervals is based on the minimum distance between faults in the two study areas (scale of mapping) and the furthest distance from a fault at which landslides have occurred. The effect of fault weakening typically occurs within close proximity to faults and decreases substantially with distance. Hence, smaller class sizes (5 km) are used close to faults, with larger classes (10 km) as distance increases beyond 10 km.

In both events the frequency ratio was highest immediately adjacent to active faults and decreased rapidly with distance (Figure 3). The spatial density of mapped active faults appears to affect the maximum distance

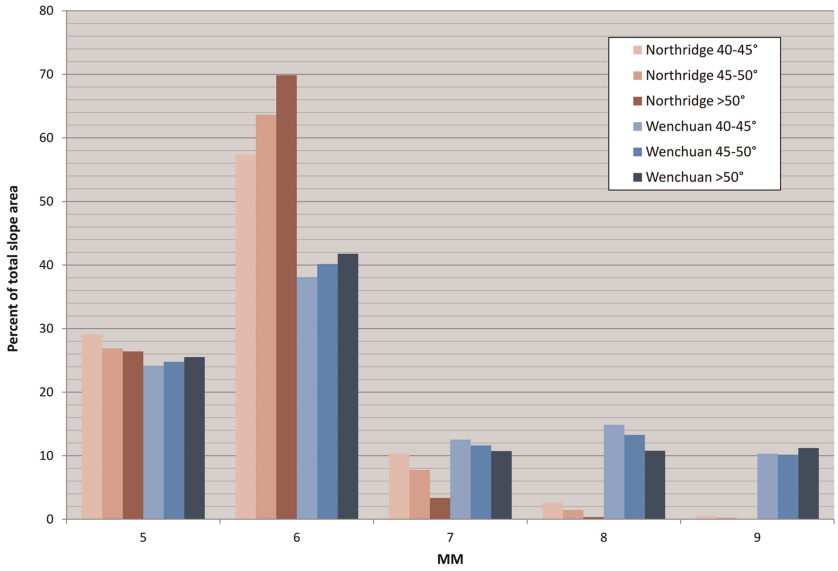

Figure 4. Distribution of slope angles >40° with respect to MM in the Northridge and Wenchuan earthquakes.

at which landslides occur. Both events show similar frequency ratio distributions, with the influence of mapped active faults becoming negligible beyond ~10 km (Figure 3).

4.1.2.3. Proximity to Streams

The role of river incision on hillslope processes and landscape evolution has been discussed in numerous studies [*Snyder et al.,* 2000; *Whipple*, 2004 *Korup*, 2004; *Larsen and Montgomery*, 2012]. Fluvial undercutting, causing high shear stresses due to removal of lateral support, has been identified as a key triggering mechanism of aseismic slope instability [*Korup*, 2004]. Therefore, proximity to drainage network has been used in many landslide studies as a conditioning factor. By including distance to streams, localized processes such as terrain modified by gully erosion [*Dai and Lee*, 2002; *Dai et al.,* 2001], stream flow undercutting [*Donati and Turrini*, 2002; *Saha et al.,* 2002 *Van Westen et al.,* 2003], and headward stream channel erosion [*He and Beighley*, 2008] can be accounted for.

Herein, streams are derived using a flow accumulation tool within the GIS, with a stream assumed to form when the contributing catchment area exceeds 1 km^2. Distance from streams is then computed as the horizontal distance from the center of the resulting stream channel. Distance from streams is classified using equal-sized classes of 0.5 km, based on the drainage network densities in Northridge and Wenchuan and the spatial resolution of the DEMs.

Both events show generally decreasing frequency ratio with increasing distance (Figure 3), with areas within 1.5 km of a stream producing the largest proportion of landslides. The small differences in landslide frequency ratio between Wenchuan and Northridge are perhaps associated with the different uplift rates and consequent fluvial erosion rates. Additionally, in Wenchuan there are significantly more powerful stream channels compared to Northridge that may affect the landscape at greater distances. Nevertheless, distance from streams plays an important role in both events with the highest landslide densities being observed within 1 km and substantially decreasing at >1.5 km.

4.1.2.4. Slope Position

One of the key factors favoring coseismic landsliding is the amplification of seismic ground motion by topography, known as topographic amplification [*Meunier et al.,* 2008]. This is a localized increase in the ground motion amplitude generated by the propagation of seismic waves on the Earth's surface and through the crust. This has received increased attention over the last few decades [*Davis and West*, 1973; *Spudich et al.,* 1996; *Athanasopoulos et al.,* 1999; *LeBrun et al.,* 1999; *Havenith et al.,* 2003; *Wald and Allen*, 2007; *Meunier et al.,* 2008; *Buech et al.,* 2010] showing that different parts of hillslopes (e.g., ridge, midslope, and base) respond differently to seismic shaking. Despite the progress in understanding the phenomenon at the local scale, limited studies have attempted to model topographic amplification at the regional scale [*Lee et al.,* 2008, 2009a, 2009b].

To classify the landscape according to relative slope position, we use the Topographic Position Index (TPI) [*Weiss*, 2001]. This compares the elevation of each cell in a DEM to the mean elevation of a specified neighborhood around that cell. The output is a continuous raster where positive TPI values represent locations that are higher than the average of their surroundings (e.g., ridges) and negative values represent lower locations (e.g., valleys). TPI values near zero are areas of uniform slope angle. This can then be classified into various discrete slope position classes [*Jenness et al.,* 2013]. Herein, we classify the landscape into four slope position classes (valleys, midslopes, ridges, and flat plains) following the example given in *Jenness et al.* [2013].

The highest landslide frequency ratios are observed at ridges in both environments (Figure 3). This agrees with *Buech et al.* [2010] who showed that ground shaking was amplified most along ridgelines thus increasing the probability of slope failure. Frequency ratio generally decreases as slope class changes to midslopes, valleys, and flat plains (Figure 3). In Wenchuan the density of landslides at midslopes is similar to that in valleys, probably because *Gorum et al.* [2011] mapped lateral spreads which occurred at river banks within valleys, increasing the frequency ratio for this class. Lateral spreads were not mapped in the Northridge inventory [*Harp and Jibson*, 1996]. Nevertheless, midslopes show a marked reduction in frequency ratio at Northridge. This is likely a result of a small number of pixels being classified as midslopes because elevation in the region is limited to ~2700 m resulting in relatively short slopes with continuous slope angle when using a 60 m DEM. In Wenchuan, the maximum elevation is ~6000 m resulting in significantly longer slopes and thus more pixels classified as midslopes.

4.1.2.5. Other Factors

Slope aspect influenced the location of landslides in both Northridge and Wenchuan but did not correlate across the events (Figure 3). Landslides in Northridge favored south facing to west facing slopes [*Harp and Jibson*, 1996], while in Wenchuan they favored south facing to east facing slopes (Figure 3). This is likely an effect of slope orientation in relation to seismic wave propagation, a factor which may yield useful results but is beyond the scope of this study. Slope curvature appeared to play no significant role in landslide formation; both convex and concave slopes had similar effects and were only slightly more influential than flat slopes (Figure 3).

No geotechnical factors describing the strength of the underlying materials were analyzed in this study. Although geotechnical properties of slope material have previously been identified as influencing coseismic landslides, they vary greatly even within the same study area, both between and within geologic units [*Dreyfus et al.,* 2013]. Accurate measurement of these properties at enough sites to allow meaningful quantification of their regional variation is often not feasible. Further, statistical analysis can only consider factors that are present in the study areas. Therefore, considering geotechnical properties results in the method being inapplicable beyond its study region. This study attempts to develop a method that is not limited to a single study area and can be applied where geotechnical data are not available; it therefore does not consider geotechnical data. While such data undoubtedly influence landslide occurrence, including them herein will limit the method to only the Northridge and Wenchuan regions. Nevertheless, if such data sets are available and their effect known, these can be incorporated into this method to increase the accuracy and robustness of the results.

4.1.3. Fuzzy Memberships and Aggregation

To enable regional-scale modeling, fuzzy membership functions are created based on the landslide frequency ratio distributions for the factors described above (Figure 5). In order to fit membership curves to the frequency ratio data, we employ the coefficient of determination (R^2) to achieve a "best fit" for the data. To account for any inconsistencies within the data, these best fit curves are, if necessary, subjectively altered to better represent the inferred influence of that factor. For instance, the membership curve for slope angle in Wenchuan is manually altered from the data-driven best fit curve to produce smaller memberships in low slope angles. This is in order to account for the presence of lateral spreads in this inventory, which are not present in the Northridge inventory (but may have occurred) (Figure 3).

The resulting membership functions transform the input factors to a 0 to 1 scale (Figure 5) representing the relative influence on landslide occurrence of the corresponding factor. The resulting fuzzy factor maps are aggregated via fuzzy Gamma overlay to yield the hazard map for each region (Figures 1 and 6). These maps quantitatively show the relative probability of landsliding from 0 to 1 for each pixel in the study area.

To determine the appropriate γ value, the average relative probabilities of three randomly selected pixels corresponding to known landslide locations and three corresponding to flat ground with no landslides (flat areas in MM V) are compared [see *Kritikos and Davies*, 2014**]**. The values of γ between 0.8 and 0.9 provide

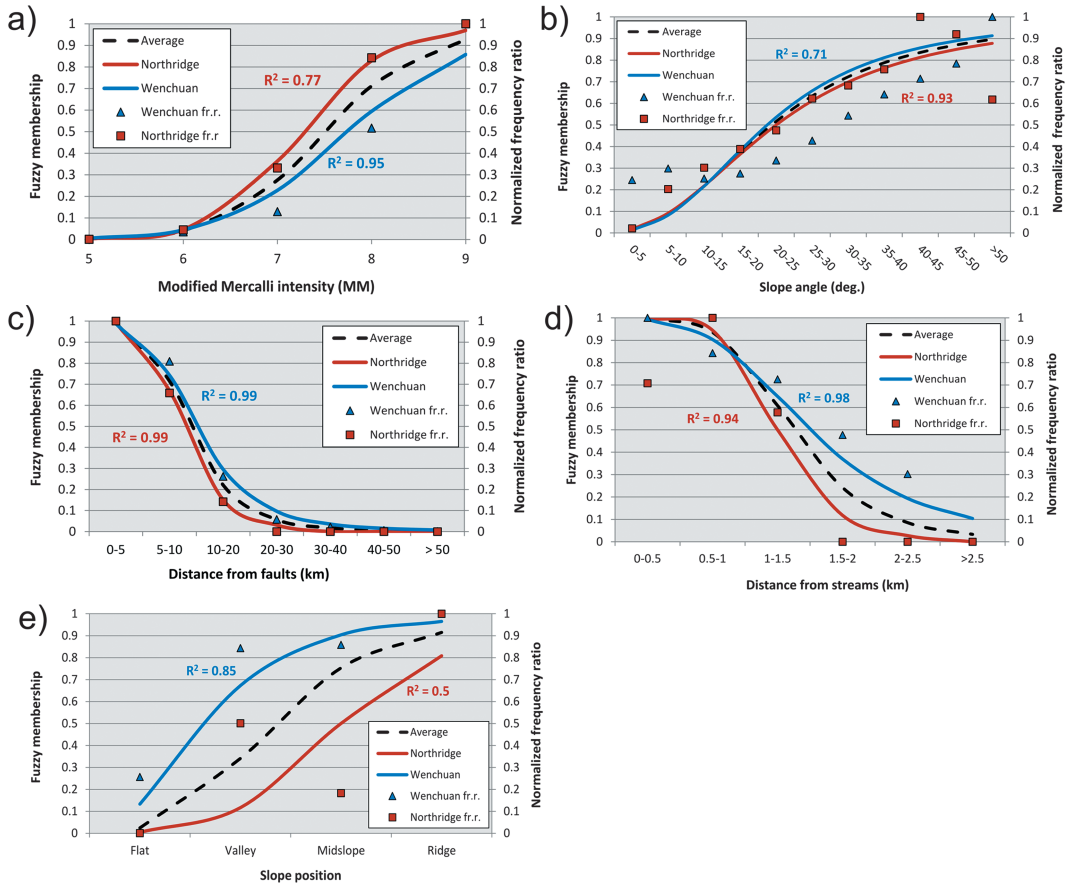

Figure 5. Earthquake specific and combined (average) fuzzy membership curves developed for (a) shaking intensity (MM), (b) slope angle, (c) distance from faults, (d) distance from streams, and (e) slope position. Points show normalized frequency ratio (fr.r.) data for each class (see Figure 3).

the best compromise between achieving high susceptibility values at known landslide locations and low values at locations known not to have sustained landsliding (Figure 7). Herein we use a value of 0.9 as this achieves comparatively marginally higher hazard values for the same landslide pixel, and when undertaking scenario analysis it is preferential to overestimate hazard than underestimate. The Wenchuan model was also undertaken using $\gamma = 0.8$ with only negligible difference in success rate (see below).

To apply this model in other locations (i.e., Chi-Chi), we first develop fuzzy memberships specific to each earthquake (i.e., only using the frequency ratios from the corresponding earthquake) before combining these to derive average membership functions (Figure 5) that can be applied to other regions. Both the earthquake-specific and average membership functions are then applied to the Northridge and Wenchuan events (Figure 6) and evaluated to demonstrate that there is no meaningful loss in accuracy using the average memberships. The difference maps show the difference in corresponding pixel values between the two maps. For both locations it is notable that the differences in pixel values are generally small; the average membership results are not significantly different from the earthquake-specific results. In Northridge, the average memberships primarily result in slightly decreased pixel values compared to the earthquake-specific memberships, while in Wenchuan they result in slightly increased values. In order to evaluate the effect of this, quantitative evaluation is required.

4.2. Evaluation

Landslide hazard analyses require some form of assessment to evaluate their accuracy and reliability before they are used in practice. The aim of the evaluation stage is (i) to assess how successfully the aggregation of the selected factors predicts the spatial distribution of landslides and (ii) to investigate whether the average memberships result in a meaningful loss in model performance.

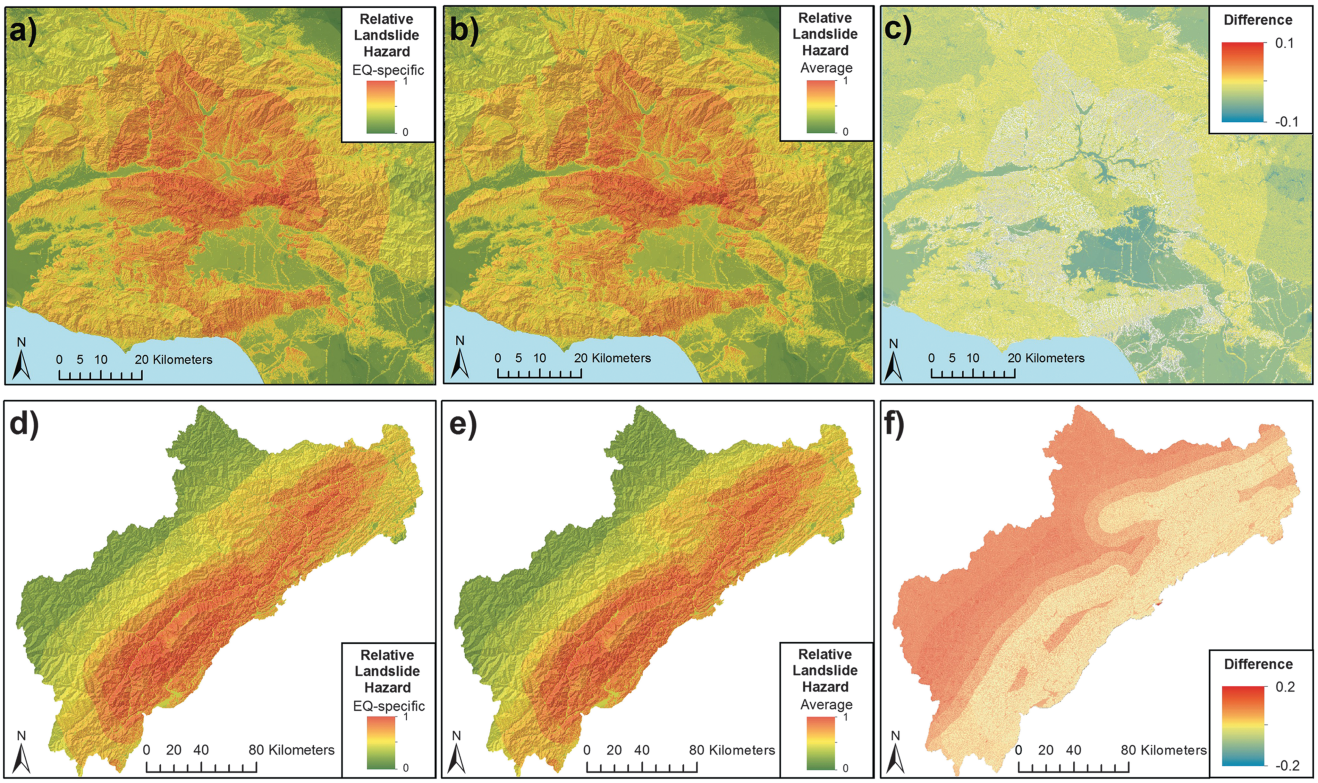

Figure 6. Modeled coseismic landslide hazard for (a–c) Northridge and (d–f) Wenchuan showing results derived from earthquake-specific membership curves (Figures 6a and 6d), average membership curves (Figures 6b and 6e), and difference in pixel values between the models (Figures 6c and 6f).

A commonly applied technique to evaluate the output is the construction of success rate curves [*Chung and Fabbri*, 1999; *Van Westen et al.,* 2003; *Remondo et al.,* 2003b; *Frattini et al.,* 2010]. For these, the output pixel values are binned into 100 equal intervals and the number of landslides in each interval is summed [*Miles and Keefer*, 2009a]. Success curves therefore compare the proportion of total landslides (*y* axis) to the proportion of predictive values (bins) they occur in (*x* axis) from highest to lowest values. The area under the curve (AUC) defines the performance (or success rate), with values of 0.5 being no better than random and values of 1.0 reflecting perfect performance. Generally, AUCs above 0.7 are considered good and the model is deemed successful. In order to assess the model's predictive capability, rather than how well the model fits the data (goodness of fit), the test data set is used, not the training data set on which statistical analysis was undertaken (see above). First, we calculate the AUC using the entire study area, before comparing this result with only those predicted hazard values on slopes $>5°$. Slopes below this are highly unlikely to produce landslides (Figures 3 and 5) and thus have correspondingly low hazard values (Figure 6). Including these slopes may artificially increase the AUC value. Removing them from the evaluation provides a better test of whether the method is able to successfully predict landslide hazard in the area where landsliding can occur.

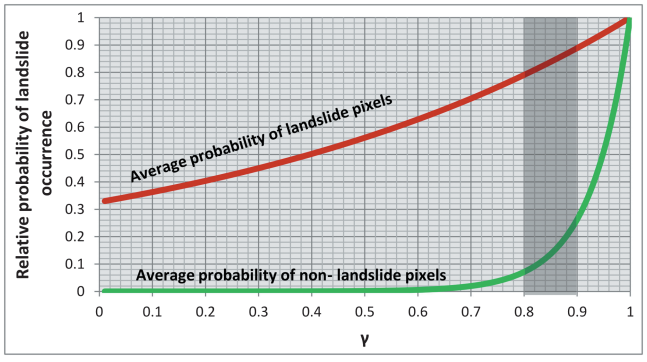

Figure 7. Effect of different γ values on the predicted hazard for three randomly selected pixels corresponding to known landslide locations and three corresponding to flat ground with no landslides in Wenchuan. Shaded box shows the range of γ values that provide the best trade-off between high values for known landslide pixels and low values for nonlandslide pixels.

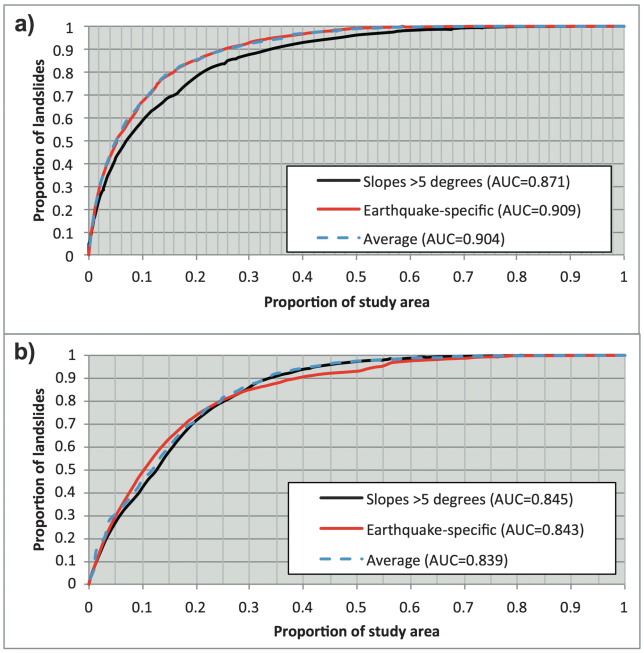

Figure 8. Success rate curves for the (a) Northridge and (b) Wenchuan earthquakes comparing the earthquake-specific and average memberships for the total study area and the area with slope angles >5°.

For Northridge the earthquake-specific memberships achieve an AUC of 0.909 and in Wenchuan an AUC of 0.843 for the entire study area (Figure 8). In comparison the average memberships achieve an AUC of 0.904 for Northridge and 0.839 for Wenchuan for the entire study area (Figure 8). Thus, there is very little loss in accuracy when using the average memberships. When considering only the area with slopes >5°, the average memberships achieve AUC of 0.871 for Northridge and 0.845 for Wenchuan. The reduced success in Northridge is likely a result of large areas with slopes <5° being removed, while in Wenchuan, only a very small portion of the study area consists of such slopes. Furthermore, using $\gamma = 0.8$ for Wenchuan with average membership curves across the entire study area achieves an AUC of 0.838, suggesting that the model is not sensitive to changes in γ between 0.8 and 0.9. All AUC values indicate that the model is successful.

4.3. Sensitivity Analysis

Sensitivity analysis is performed in order to assess the sensitivity of the hazard models to changes in the input data. It used different factor combinations and evaluated any resulting change in predictive performance of each model. For each environment five models are initially tested by excluding one factor in each trial and calculating the new AUC. A lower performance compared to the initial model indicates that the excluded factor is necessary. Conversely, if the removal of the factor results in the same or higher predictive performance, the factor is considered redundant (Table 2).

The sensitivity analysis results indicate that the exclusion of proximity to streams and slope position marginally increases the AUC in both environments (Table 2), suggesting they are redundant. However, a successful output in terms of AUC may not always be realistic in terms of physical meaning. Figure 9 shows the difference in the Northridge hazard maps when removing the distance from streams and slope position factors from the model. The higher susceptibility observed in the flat areas is unrealistic and primarily a result of the absence of the slope position factor. Slope position is therefore assumed to be a necessary factor to achieve realistic physical meaning and is retained because it achieves more realistic results, albeit with a smaller AUC than is possible (Table 2).

Table 2. AUC Values of Different Factor Combinations for Northridge and Wenchuan

	Northridge	Wenchuan	
Input Factors	AUC		Factors Excluded
Ground shaking intensity, slope angle, proximity to active faults, proximity to streams, and slope position	0.909	0.843	-
Slope angle, proximity to active faults, proximity to streams, and slope position	0.769	0.785	Ground shaking intensity
Ground shaking intensity, proximity to active faults, proximity to streams, and slope position	0.878	0.799	Slope angle
Ground shaking intensity, slope angle, proximity to streams, and slope position	0.904	0.825	Proximity to active faults
Ground shaking intensity, slope angle, proximity to active faults, and slope position	0.911	0.843	Proximity to streams
Ground shaking intensity, slope angle, proximity to active faults, and proximity to streams	0.918	0.845	Slope position
Ground shaking intensity, slope angle, and proximity to active faults	0.912	0.851	Proximity to streams and slope position

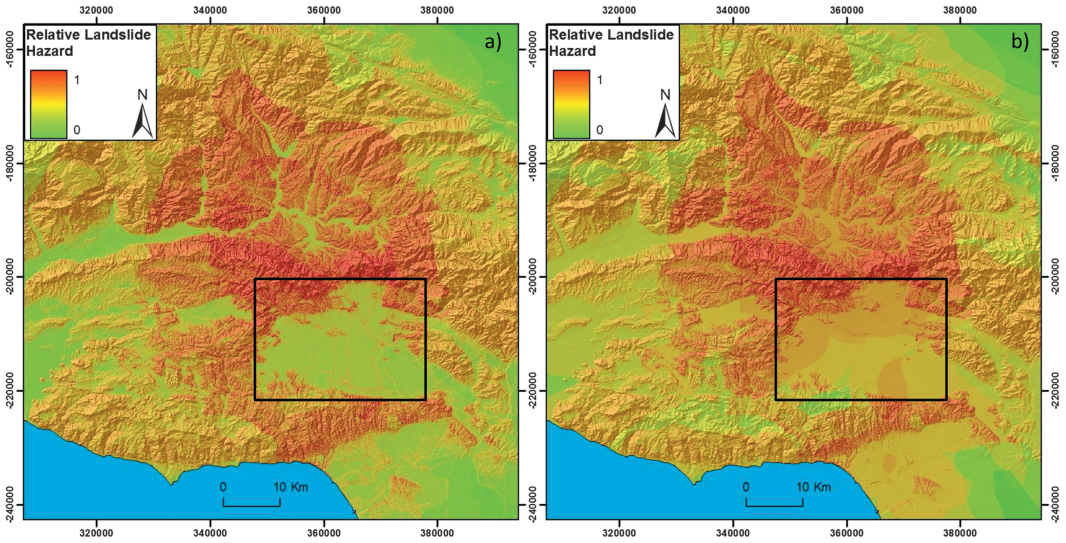

Figure 9. Difference in hazard maps for Northridge between the (a) initial model and (b) three-parameter model excluding proximity to streams and slope position factors. Black rectangle shows the unrealistic increased hazard on the flat ground as a result of the removal of the slope position factor.

4.4. Predictive Scenario Analysis

To show that the average memberships for these four factors (MM, slope angle, slope position, and proximity to active faults) can successfully predict landslide hazard beyond the Northridge and Wenchuan regions, accurate modeling (i.e., AUC $>$ 0.7) of another historic earthquake with a comprehensive coseismic landslide inventory is required. We do this by applying the average membership values to the 1999 Chi-Chi earthquake. The resulting hazard map and success curves are shown in Figure 10. The result is an AUC of 0.921 for the entire study area, which corresponds to ~90% of observed landslides occurring in the 20% of highest predicted hazard values. Again, we compare this with the success rate for the area with slopes $>$5°, which achieves an AUC of 0.915. Thus, the average membership curves derived from the Northridge and Wenchuan inventories are able to successfully predict the landslide hazard from the Chi-Chi earthquake despite using only an isoseismal map, DEM, and active faults map of the region. This suggests that the model derived herein could be applied to earthquake scenarios in other locations where a 60 m DEM and active fault map are available, but comprehensive geotechnical data and historic inventories are not, and achieve meaningful results in terms of coseismic landslide hazard. The present model thus exceeds the capability of previous models, which cannot be used in such cases.

5. Discussion

This work demonstrates that the coseismic landslide hazard (the relative probability of a landslide occurring at a given location for a given event) for any given earthquake scenario can be adequately modeled using memberships derived from other regions. This is important for hazard analysis in mountainous regions with seismic hazard that have no historical coseismic landslide inventories or geotechnical data (e.g., the Southern Alps of New Zealand). The Chi-Chi scenario analysis above demonstrates that it is possible to establish accurate and realistic hazard maps prior to an earthquake; if a DEM, active faults map and scenario isoseismals can be produced.

While the current memberships have been shown to be successful beyond their training regions, it is not known how applicable they are to regions with substantially different environments, for example, heavily glaciated environments such as Denali, Alaska, or the high Himalaya. The presence of large glaciers and thick ice accumulation zones may fundamentally alter the factors which control spatial distribution [e.g., *McColl et al.,* 2012], and therefore, historic landslide inventories from events in such regions (e.g., 2002 M_w 7.8 Denali earthquake [see *Gorum et al.,* 2014]) should be investigated to establish their applicability. Applying the model in only three different environments and achieving high success rates may be coincidental. However, given the number of factors considered, the markedly different environments involved, and the different seismic scenarios, we suggest it is unlikely the successful results are simply coincidence. Nevertheless,

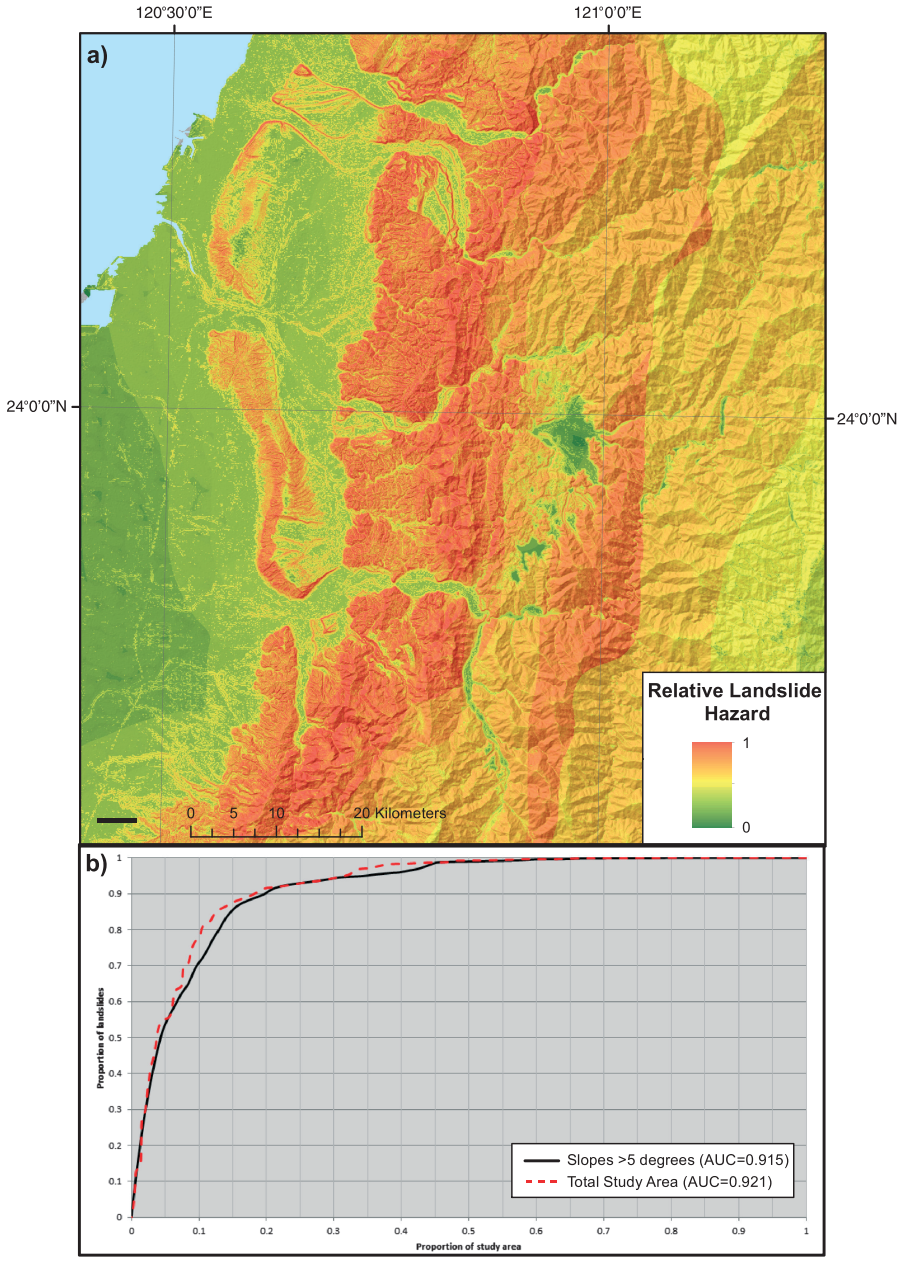

Figure 10. Predicted coseismic landslide hazard for the 1999 Chi-Chi earthquake and the associated success curves.

coseismic landslide inventories from other locations should be investigated when they become available, to further test and train the model. This will increase the robustness of the memberships included and may identify further influencing factors that can be incorporated into the model.

As with all GIS-based statistical methods, the model is particularly sensitive to the quality and accuracy of the landslide inventories and the input information layers. The inventory quality, which depends on the accuracy of landslide mapping, is crucial to both training and evaluation stages as the spatial correlation between landslides and individual factors is the fundamental component of the model. The timing of the landslide mapping after the earthquake may also significantly affect the model's output. If the inventory includes slope failures that occurred before the main shock, during the aftershock sequence or in postevent rainfalls, the model will overestimate the landslide density and consequently result in unrealistic fuzzy memberships. An example is the Chi-Chi landslide inventory used herein which may include landslides that occurred before the

earthquake according to recent studies [*Lee*, 2013, 2014] that demonstrate the earthquake likely generated ~13,000 landslides. The issue of input data quality is further complicated when information from different environments is combined. The resolutions of the various data layers must be the same and should match the scale of the assessment (e.g., regional-scale input data will only provide a useful output for a regional-scale study); otherwise, the model's predictive capability will be significantly decreased.

Another limitation results from the use of oversimplified input data by only considering information that is relatively easily mapped or derived from a DEM. For instance, the influence of topographic amplification is modeled based on the TPI [*Weiss*, 2001] to classify the landscape according to relative slope positions. This is a simplification of a very complex phenomenon at regional scale. It does not take into account other parameters such as the orientation of topographic irregularities with respect to the ground motion, resonant frequencies, or sharp contrasts of mechanical properties with depth or between geological formations. Additionally, the TPI is an inherently scale-dependent parameter; at a 50 m scale a point might be considered a flat plain whereas at a scale of several kilometres this same point might be at the bottom of a steep valley [*Jenness et al.,* 2013]. Therefore, the slope positions identified by this technique depend entirely on the scale of the analysis and the resolution of the DEM. This may be the reason why removing slope position factor results in slightly increased AUC values as it is too simplified at the regional scale.

Reclassifying continuous data of landslide causative factors (e.g., slope angle) into discrete classes is necessary in order to calculate the distribution of landslide density for each factor. This process introduces a degree of subjectivity and a source of uncertainty in the modeling approach. Since the shapes of the fuzzy membership curves are related to the distributions of landslide densities, the size and number of classes within a factor can directly affect the result. To minimize the effect of this source of uncertainty the size and number of classes are selected based on the mapping scale of each factor (e.g., mapping scale of active faults map), the DEM resolution and the spatial distribution of landslides within the factor (e.g., closest and farthest distances from a fault or stream where landslides are observed). However, the most important step to minimize the uncertainties of class boundaries is the application of semi data-driven fuzzy memberships. The shapes of the membership curves are fitted to landslide densities from the inventory data using the coefficient of determination (R^2). This allowed us to alter the shape of a curve to account for any known errors or inconsistencies within the data and maintain a high R^2 at the same time. By doing this, the landslide density distributions with discrete class boundaries are transformed into continuous fuzzy membership curves with a similar shape and no discrete boundaries. However, this process also involves a degree of subjectivity that can directly affect the final output.

These considerations suggest that the predictive ability of the present model must be taken as an order-of-magnitude estimate only. Nevertheless, in regions with no historic or geotechnical data, such estimates are useful for preliminary hazard assessment and mitigation planning.

6. Conclusions

This study (i) identifies factors common to multiple regions that appear to influence coseismic landslide occurrence to the same extent, (ii) models the influence of these factors using fuzzy logic in GIS, and (iii) demonstrates that these factors can be used to successfully assess landslide hazard beyond the study areas. In particular

1. Landslide inventories from the 1994 Northridge and 2008 Wenchuan earthquakes reveal four factors demonstrating strong correlation across both events: shaking intensity (MM), slope angle, distance from active faults, and slope position.
2. Based on the frequency ratio of observed landslides within these factors, semi data-driven average membership curves are developed to successfully model the coseismic landslide hazard for both events.
3. These memberships are successfully applied to the 1999 M_w7.7 Chi-Chi earthquake. The results show that 90% of the landslides in the Chi-Chi event occurred in the highest 20% of modeled hazard values, showing that the method can be applied with meaningful accuracy beyond the Northridge and Wenchuan regions.

Analysis of other available coseismic landslide inventories can increase the robustness of the membership curves and identify other factors that may potentially influence landsliding similarly across multiple environments. The present method, and the memberships derived, allows preliminary hazard analyses in regions with the potential for coseismic landsliding, for which quantitative analysis has not previously been possible.

Acknowledgments
The landslide inventory for Wenchuan earthquake was kindly provided to us by Tolga Gorum of ITC, University of Twente, Netherlands. The landslide inventory for Chi-Chi earthquake was provided by Hongey Chen of National Taiwan University, Taiwan. Northridge landslide data set is publically available from the U.S. Geological Survey at: http://earthquake.usgs.gov/earthquakes/shakemap/sc/shake/Northridge/#download. We also wish to thank Alex Densmore and the three anonymous reviewers for their constructive review and insightful comments that helped us improve this manuscript.

References

Agterberg, F. P., and Q. Cheng (2002), Conditional independence test for weights of evidence modelling, *Nat. Resour. Res.*, *11*, 249–255.
Aleotti, P., and R. Chowdhury (1999), Landslide hazard assessment: Summary review and new perspectives, *Bull. Eng. Geol. Environ.*, *58*, 21–44.
Athanasopoulos, G. A., P. C. Pelekis, and E. A. Leonidou (1999), Effects of surface topography on seismic ground response in the Egion (Greece) 15 June 1995 earthquake, *Soil Dyn. Earthquake Eng.*, *18*(2), 135–149.
Beyer, H. L. (2004), Hawth's analysis tools for ArcGIS. [Available at http://www.spatialecology.com/htools.]
Bonham-Carter, G. F. (1994), *Geographic Information Systems for Geoscientists*, Pergamon, Ottawa.
Bray, J. D., and T. Travasarou (2009), Pseudostatic coefficient for use in simplified seismic slope stability evaluation, *J. Geotech. Geoenviron. Eng.*, *135*, 1336–1340.
Brune, J. N. (2001), Shattered rock and precarious rock evidence for strong asymmetry in ground motions during thrust faulting, *Bull. Seismol. Soc. Am.*, *91*, 441–447.
Buech, F., T. R. Davies, and J. R. Pattinga (2010), The little red hill seismic experimental study: Topographic effects on ground motion at a bedrock-dominated mountain edifice, *Bull. Seismol. Soc. Am.*, *100*(5A), 2219–2229, doi:10.1785/0120090345.
Carrara, A., M. Cardinali, R. Detti, F. Guzzetti, V. Pasqui, and P. Reichenbach (1991), GIS techniques and statistical models in evaluating landslide hazard, *Earth Surf. Processes Landform*, *16*, 427–445.
Carrara, A., M. Cardinali, F. Guzzetti, and P. Reichenbach (1995), GIS technology in mapping landslide hazard, in *Geographical Information Systems in Assessing Natural Hazards*, edited by A. Carrara and F. Guzzetti, pp. 135–175, Kluwer Acad., Dordrecht, Netherlands.
Chi, W.-C., D. Dreger, and A. Kaverina (2001), Finite-source modeling of the 1999 Taiwan (Chi-Chi) Earthquake derived from a dense strong-motion network, *Bull. Seismol. Soc. Am.*, *91*, 1144–1157.
Chigira, M., W. Wang, T. Furuya, and T. Kamai (2003), Geological causes and geomorphological precursors of the Tsaoling landslide triggered by the 1999 Chi-Chi earthquake, Taiwan, *Eng. Geol.*, *68*(3), 259–273.
Chung, C. F., and A. G. Fabbri (1999), Probabilistic prediction models for landslide hazard mapping, *Photogramm. Eng. Remote Sens.*, *65*(12), 1389–1399.
Clough, R. W., and A. K. Chopra (1966), Earthquake stress analysis in earth dams, *ASCE J. Eng. Mech. Div.*, *92*, 197–211.
Crozier, M. J., and T. Glade (2005), Landslide hazard and risk: Issues, concepts and approach, in *Landslide Risk Assessment*, edited by T. Glade, M. G. Anderson, and M. J. Crozier, pp. 1–40, John Wiley, Chichester, U. K.
Cui, P., Y. Zhu, Y. Han, X. Chen, and J. Zhuang (2009), The 12 May Wenchuan earthquake-induced landslide lakes: Distribution and preliminary risk evaluation, *Landslides*, *6*(3), 209–223.
Dadson, S., et al. (2004), Earthquake-triggered increase in sediment delivery from an active mountain belt, *Geology*, *32*(8), 733–736.
Dai, F. C., and C. F. Lee (2002), Landslide characteristics and, slope instability modeling using GIS, Lantau Island, Hong Kong, *Geomorphology*, *42*(3–4), 213–228.
Dai, F. C., C. F. Lee, J. Li, and Z. W. Xu (2001), Assessment of landslide susceptibility on the natural terrain of Lantau Island, Hong Kong, *Environ. Geol.*, *40*(3), 381–391.
Dai, F. C., C. Xu, X. Yao, L. Xu, X. B. Tu, and Q. M. Gong (2010), Spatial distribution of landslides triggered by the 2008 M_s 8.0 Wenchuan earthquake, China, *J. Asian. Earth Sci.*, *40*, 883–895.
Davis, L. L., and L. R. West (1973), Observed effects of topography on ground motion, *Bull. Seismol. Soc. Am.*, *63*, 283–298.
Del Gaudio, V., and J. Wasowski (2004), Time probabilistic evaluation of seismically-induced landslide hazard in Irpinia (Southern Italy), *Soil Dyn. Earthquake Eng.*, *24*, 915–928.
Del Gaudio, V., P. Pierri, and J. Wasowski (2003), An approach to time-probabilistic evaluation of seismically induced landslide hazard, *Bull. Seismol. Soc. Am.*, *93*, 557–569.
Densmore, A., M. A. Ellis, Y. Li, R. Zhou, G. Hancock, and N. Richardson (2007), Active tectonics of the Beichuan and Pengguan faults at the eastern margin of the Tibetan Plateau, *Tectonics*, *26*, TC4005, doi:10.1029/2006TC001987.
Donati, L., and M. C. Turrini (2002), An objective method to rank, the importance of the factors predisposing to landslides with the GIS methodology: Application to an area of the Apennines, (Valnerina; Perugia, Italy), *Eng. Geol.*, *63*(3–4), 277–289.
Dramis, F., and M. Sorriso-Valvo (1994), Deep-seated gravitational slope deformation, related landslides and tectonics, *Eng. Geol.*, *38*, 231–243.
Dreyfus, D., E. M. Rathje, and R. W. Jibson (2013), The influence of different simplified sliding-block models and input parameters on regional predictions of seismic landslides triggered by the Northridge earthquake, *Eng. Geol.*, *163*, 41–54.
Dubois, D., and H. Prade (1985), A review of fuzzy set aggregation connectives, *Inf. Sci.*, *36*, 85–121.
Environmental Systems Research Institute (2011), ArcGIS desktop help 10—How fuzzy overlay works. [Available at http://help.arcgis.com/en/arcgisdesktop/10.0/help/index.html#/How_Fuzzy_Overlay_works/009z000000s0000000/, Accessed on 9/30/2011.]
Fan, X., C. J. van Westen, O. Korup, T. Gorum, Q. Xu, F. Dai, and G. Wang (2012), Transient water and sediment storage of the decaying landslide dams induced by the 2008 Wenchuan earthquake, China, *Geomorphology*, *171*, 58–68.
Frattini, P., G. Crosta, and A. Carrara (2010), Techniques for evaluating the performance of landslide susceptibility models, *Eng. Geol.*, *111*(1–4), 62–72.
Glade, T., and M. J. Crozier (2005), The nature of landslide hazard and impact, in *Landslide Hazard and Risk*, edited by T. Glade, M. Anderson, and M. Crozier, pp. 43–74, Wiley, Chichester, U. K.
Gorum, T., X. Fan, C. van Westen, R. Huang, Q. Xu, C. Tang, and G. Wang (2011), Distribution pattern of earthquake-induced landslides triggered by the 12 May 2008 Wenchuan earthquake, *Geomorphology*, *133*(3), 152–167.
Gorum, T., O. Korup, C. J. van Westen, M. van der Meijde, C. Xu, and F. D. van der Meer (2014), Why so few? Landslides triggered by the 2002 Denali earthquake, Alaska, *Quat. Sci. Rev.*, *95*, 80–94.
Guzzetti, F., A. Carrarra, M. Cardinali, and P. Reichenbach (1999), Landslide hazard evaluation: A review of current techniques and their application in a multiscale study, Central Italy, *Geomorphology*, *31*, 181–216.
Harp, E., and R. Jibson (1996), Landslides triggered by the 1994 Northridge, California, earthquake, *Bull. Seismol. Soc. Am.*, *86*(1B), S319–S332.
Harp, E. L., D. K. Keefer, H. P. Sato, and H. Yagi (2011), Landslide inventories-the essential part of seismic landslide hazard analyses, *Eng. Geol.*, *122*, 9–21.
Hauksson, E., L. Jones, and K. Hutton (1995), The 1994 Northridge earthquake sequence in California: Seismological and tectonic aspects, *J. Geophys. Res.*, *100*(B7), 12,335–12,355, doi:10.1029/95JB00865.
Havenith, H.-B., M. Vanini, D. Jongmans, and E. Faccioli (2003), Initiation of earthquake-induced slope failure: Influence of topographical and other site specific amplification effects, *J. Seismol.*, *7*, 397–412.
He, Y. P., and R. E. Beighley (2008), GIS-based regional landslide susceptibility mapping: A case study in southern California, *Earth Surf. Processes Landforms*, *33*(3), 380–393.

Hewitt, K., J. J. Clague, and J. F. Orwin (2008), Legacies of catastrophic rock slope failures in mountain landscapes, *Earth Sci. Rev.*, *87*(1), 1–38.
Huabin, W., L. Gangjun, X. Weiya, and W. Gonghui (2005), GIS based landslide hazard assessment: An overview, *Prog. Phys. Geogr.*, *29*(4), 548–567.
Jenness, J., B. Brost, and P. Beier (2013), Manual: Land facet corridor designer, p. 110.
Jibson, R. W. (2007), Regression models for estimating coseismic landslide displacement, *Eng. Geol.*, *91*, 209–218.
Jibson, R. W., E. L. Harp, and J. A. Michael (2000), A method for producing digital probabilistic seismic landslide hazard maps, *Eng. Geol.*, *58*, 271–289.
Keefer, D. K. (1984), Landslides caused by earthquakes, *Bull. Geol. Soc. Am.*, *95*, 406–421.
Kellogg, K. S. (2001), Tectonic controls on a large landslide complex: Williams Fork Mountains near Dillon, Colorado, *Geomorphology*, *41*, 355–368.
Khazai, B., and N. Sitar (2004), Evaluation of factors controlling earthquake-induced landslides caused by Chi-Chi earthquake and comparison with the Northridge and Loma Prieta events, *Eng. Geol.*, *71*, 79–95.
Korup, O. (2004), Geomorphic implications of fault zone weakening: Slope instability along the Alpine Fault, South Westland to Fiordland, *N. Z. J. Geol. Geophys.*, *47*, 257–267.
Kritikos, T., and T. Davies (2014), Assessment of rainfall-generated shallow landslide/debris-flow susceptibility and runout using a GIS-based approach: Application to western Southern Alps of New Zealand, *Landslides*, doi:10.1007/s10346-014-0533-6.
Larsen, I. J., and D. R. Montgomery (2012), Landslide erosion coupled to tectonics and river incision, *Nat. Geosci.*, *5*, 468–473.
LeBrun, B., D. Hatzfeld, P. Y. Bard, and M. Bouchon (1999), Experimental study of the ground motion on a large scale topographic hill in Kitherion (Greece), *J. Seismol.*, *3*, 1–15.
Lee, C. T. (2013), Re-evaluation of factors controlling landslides triggered by the 1999 Chi-Chi earthquake, in *Earthquake-Induced Landslides*, edited by K. Ugai, H. Yagi, and A. Wakai, pp. 213–224, Springer, Berlin.
Lee, C. T. (2014), Statistical seismic landslide hazard analysis: An example from Taiwan, *Eng. Geol.*, *182*, Part B, 201–212.
Lee, C. T., C. C. Huang, J. F. Lee, K. L. Pan, M. L. Lin, and J. J. Dong (2008), Statistical approach to earthquake-induced landslide susceptibility, *Eng. Geol.*, *100*, 43–58.
Lee, S., and B. Pradhan (2007), Landslide hazard mapping at Selangor, Malaysia using frequency ratio and logistic regression models, *Landslides*, *4*(1), 33–41.
Lee, S., and T. Sambath (2006), Landslide susceptibility mapping in the Damrei Romel area, Cambodia using frequency ratio and logistic regression models, *Environ. Geol.*, *50*(6), 847–855.
Lee, S. J., Y. C. Chan, D. Komatitsch, B.-S. Huang, and J. Tromp (2009a), Effects of realistic surface topography on seismic ground motion in the Yangminshan region (Taiwan) based upon the Spectral-Element Method and LiDAR DTM, *Bull. Seismol. Soc. Am.*, *99*(2A), 681–693.
Lee, S. J., D. Komatitsch, B.-S. Huang, and J. Tromp (2009b), Effects of topography on seismic-wave propagation: An example from northern Taiwan, *Bull. Seismol. Soc. Am.*, *99*(1), 314–325, doi:10.1785/0120080020.
Li, G., A. J. West, A. L. Densmore, Z. Jin, R. N. Parker, and R. G. Hilton (2014), Seismic mountain building: Landslides associated with the 2008 Wenchuan earthquake in the context of a generalized model for earthquake volume balance, *Geochem. Geophys. Geosyst.*, *15*, 833–844, doi:10.1002/2013GC005067.
Li, Y., et al. (2009), Geological background of Longmen Shan seismic belt and surface ruptures in Wenchuan earthquake, *J. Eng. Geol.*, *17*(1), 3–18.
Lin, C., C. Shieh, B. Yuan, Y. Shieh, S. Liu, and S. Lee (2004), Impact of Chi-Chi earthquake on the occurrence of landslides and debris flows: Example from the Chenyulan River watershed, Nantou, Taiwan, *Eng. Geol.*, *71*(1), 49–61.
Liu-Zeng, J., et al. (2009), Coseismic ruptures of the 12 May 2008, M_s 8.0 Wenchuan earthquake, Sichuan: East–west crustal shortening on oblique, parallel thrusts along the eastern edge of Tibet, *Earth Planet. Sci. Lett.*, *286*, 355–370.
McColl, S. T., T. R. H. Davies, and M. J. McSaveney (2012), The effect of glaciation on the intensity of seismic ground motion, *Earth Surf. Processes Landforms*, *37*, 1290–1301.
Meunier, P., N. Hovius, and A. J. Haines (2007), Regional patterns of earthquake-triggered landslides and their relation to ground motion, *Geophys. Res. Lett.*, *34*, L20408, doi:10.1029/2007GL031337.
Meunier, P., N. Hovius, and A. J. Haines (2008), Topographic site effects and the location of earthquake induced landslides, *Eng. Geol.*, *275*, 221–232.
Miles, S. B., and D. K. Keefer (2000), Evaluation of seismic slope-performance models using a regional case study, *Environ. Eng. Geosci.*, *6*, 25–39.
Miles, S. B., and D. K. Keefer (2007), Comprehensive areal model of earthquake-induced landslides: Technical specification and user guide, *U.S. Geol. Surv. Open-File Rep., 2007–1072*, 69 pp.
Miles, S. B., and D. K. Keefer (2009a), Evaluation of CAMEL—Comprehensive areal model of earthquake-induced landslides, *Eng. Geol.*, *104*, 1–15.
Miles, S. B., and D. K. Keefer (2009b), Toward a comprehensive areal model of earthquakeinduced landslides, *Am. Soc. Civ. Eng. Nat. Hazards Rev.*, *10*, 19–28.
Naranjo, J. L., C. J. VanWesten, and R. Soeters (1994), Evaluating the use of training areas in bivariate statistical landslide hazard analysis: A case study in Colombia, *ITC J.*, *1994–3*, 292–300.
Newmark, N. M. (1965), Effects of earthquakes on dams and embankments, *Geotechnique*, *15*, 139–159.
Parise, M., and R. W. Jibson (2000), A seismic landslide susceptibility rating of geologic units based on analysis of characteristics of landslides triggered by the January 17, 1994, Northridge, California, earthquake, *Eng. Geol.*, *58*, 251–270.
Parker, R., A. Densmore, N. Rosser, M. De Michele, Y. Li, R. Huang, S. Whadcoat, and D. Petley (2011), Mass wasting triggered by the 2008 Wenchuan earthquake is greater than orogenic growth, *Nat. Geosci.*, *4*(7), 449–452.
Petley, D. (2012), Global patterns of loss of life from landslides, *Geology*, *40*(10), 927–930.
Rathje, E. M., and G. Antonakos (2011), A unified model for predicting earthquake-induced sliding displacements of rigid and flexible slopes, *Eng. Geol.*, *122*, 51–60, doi:10.1016/j.enggeo.2010.12.004.
Rathje, E. M., and G. Saygili (2009), Probabilistic assessment of earthquake-induced sliding displacements of natural slopes, *Bull. N. Z. Soc. Earthquake Eng.*, *42*, 18–27.
Remondo, J., A. González-Díez, J. R. Diaz De Terán, and A. Cendrero (2003a), Landslide susceptibility models utilising spatial data analysis techniques. A case study from the lower Deba Valley, Guipúzcoa (Spain), *Nat. Hazards*, *30*(3), 267–279.
Remondo, J., A. Gonzalez, J. R. Diaz De Terán, A. Cendrero, A. Fabbri, and C.-J. F. Chung (2003b), Validation of landslide susceptibility maps; Examples and applications from a case study in northern Spain, *Nat. Hazards*, *30*(3), 437–449.
Robinson, T. R., and T. R. H. Davies (2013), Review article: Potential geomorphic consequences of a future great (M_w = 8.0+), Alpine Fault earthquake, South Island, New Zealand, *Nat. Hazards Earth Syst.Sci.*, *13*(9), 2279–2299.

Ross, T. (1995), *Fuzzy Logic With Engineering Applications*, McGraw-Hill, New York.
Saha, A. K., R. P. Gupta, and M. K. Arora (2002), GIS-based landslide hazard zonation in the Bhagirathi (Ganga) Valley, Himalayas, *Int. J. Remote Sens.*, *23*(2), 357–369.
Saygili, G., and E. M. Rathje (2008), Empirical predictive models for earthquake-induced sliding displacements of slopes, *J. Geotech. Geoenviron. Eng.*, ASCE, *134*(6), 790–803.
Shin, T., and T. Teng (2001), An overview of the 1999 Chi-Chi, Taiwan, earthquake, *Bull. Seismol. Soc. Am.*, *91*(5), 895–913.
Snyder, N. P., K. X. Whipple, G. E. Tucker, and D. J. Merritts (2000), Landscape response to tectonic forcing: Digital elevation model analysis of stream profiles in the Mendocino triple junction region, northern California, *Geol. Soc. Am. Bull.*, *112*, 1250–1263.
Soeters, R., and C. J. Van Westen (1996), Slope stability: Recognition, analysis and zonation, in *Landslides: Investigation and Mitigation, Transportation Research Board, National Research Council Special Report 247*, edited by A. K. Turner and R. L. Shuster, pp. 129–177.
Spudich, P., M. Hellweg, and W. H. K. Lee (1996), Directional topographic site response at Tarzana observed in aftershocks of the 1994 Northridge, California, earthquake: Implications for mainshock motions, *Bull. Seismol. Soc. Am.*, *86*, 193–208.
Stewart, J. P., T. F. Blake, and R. A. Hollingsworth (2003), A screen analysis procedure for seismic slope stability, *Earthquake Spectra*, *19*, 697–712.
Terzhagi, K. (1950), Mechanism of landslides, in *Application of Geology to Engineering Practice (Berkey Volume)*, edited by S. Paige, pp. 83–123, Geol. Soc. of Am., New York.
Van Westen, C. J., N. Rengers, M. T. J. Terlien, and R. Soeters (1997), Prediction of the occurrence of slope instability phenomena through GIS-based hazard zonation, *Geol. Rundsch.*, *86*, 404–414.
Van Westen, C. J., N. Rengers, and R. Soeters (2003), Use of geomorphological information in indirect landslide susceptibility assessment, *Nat. Hazards*, *30*(3), 399–419.
Van Westen, C. J., T. W. J. Van Asch, and R. Soeters (2006), Landslide hazard and risk zonation: Why is it still so difficult?, *Bull. Eng. Geol. Environ.*, *65*, 167–184.
Varnes, D. J., and IAEG Commission on Landslides and other Mass–Movements (1984), *Landslide Hazard Zonation: A Review of Principles and Practice*, p. 63, UNESCO Press, Paris.
Wald, D., and T. Heaton (1994), A dislocation model of the 1994 Northridge, California, earthquake determined from strong ground motions, *U.S. Geol. Surv. Open File Rep.*, *94–278*.
Wald, D. J., and T. I. Allen (2007), Topographic slope as a proxy for seismic site conditions and amplification, *Bull. Seismol. Soc. Am.*, *97*(5), 1379–1395, doi:10.1785/0120060267.
Wang, F., Q. Cheng, L. Highland, M. Miyajima, H. Wang, and C. Yan (2009), Preliminary investigation of some large landslides triggered by the 2008 Wenchuan earthquake, Sichuan Province, China, *Landslides*, *6*(1), 47–54.
Wang, W. N., H. Nakamura, and S. Tsuchiya (2002), Distributions of landslides triggered by the Chi-Chi Earthquake in central Taiwan on September 21, 1999, *Landslides*, *38*, 1826.
Warr, L. N., and S. Cox (2001), Clay mineral transformations and weakening mechanisms along the Alpine Fault, New Zealand, in *The Nature and Tectonic Significance of Fault Zone Weakening, Geol. Soc. London Spec. Publ.*, vol. 186, edited by R. E. Holdsworth et al., pp. 85–101.
Wasowski, J., D. K. Keefer, and C.-T. Lee (2011), Toward the next generation of research on earthquake-induced landslides: Current issues and future challenges, *Eng. Geol.*, *122*, 1–8, doi:10.1016/j.enggeo.2011.06.001.
Weiss, A. D. (2001), Topographic position and landforms analysis. Poster presentation, ESRI User Conference, San Diego, Calif.
Whipple, K. X. (2004), Bedrock rivers and the geomorphology of active orogens, *Annu. Rev. Earth Planet. Sci.*, *32*, 85–151.
Xu, C. (2014), Preparation of earthquake-triggered landslide inventory maps using remote sensing and GIS technologies: Principles and case studies, *Geosci. Frontiers*, doi:10.1016/j.gsf.2014.03.004.
Xu, X., X. Wen, G. Yu, G. Chen, Y. Klinger, J. Hubbard, and J. Shaw (2009), Coseismic reverse-and oblique-slip surface faulting generated by the 2008 M_w 7.9, Wenchuan earthquake, China, *Geology*, *37*(6), 515–518.
Yilmaz, I. (2009), Landslide susceptibility mapping using frequency ratio, logistic regression, artificial neural networks and their comparison: A case study from Kat landslides (Tokat—Turkey), *Comput. Geosci.*, *35*(6), 1125–1138.
Yu, S., H. Chen, and L. Kuo (1997), Velocity field of GPS stations in the Taiwan area, *Tectonophysics*, *274*(1), 41–59.
Zadeh, L. A. (1965), Fuzzy sets, *Inf. Control*, *8*, 338–353.
Zimmermann, H. J. (1991), *Fuzzy Set Theory and Its Applications*, p. 399, Kluwer Acad., Boston.